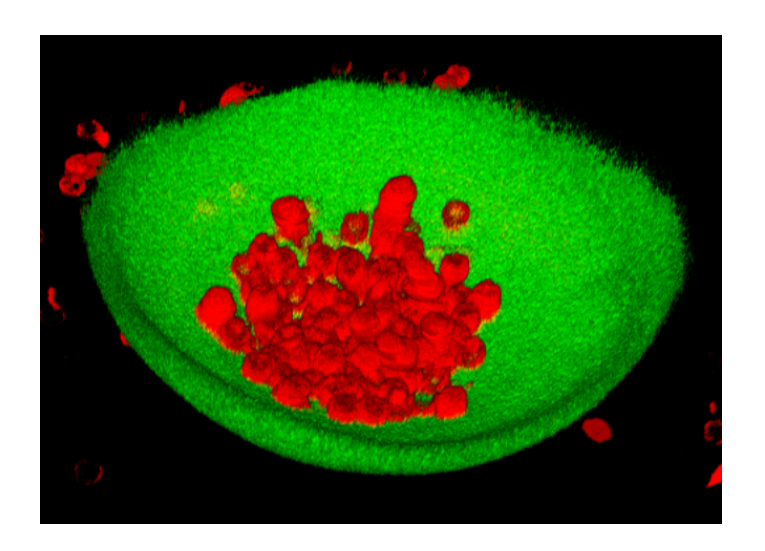


The effect of curvature on diffusion in solid supported lipid bilayers



 $\begin{array}{cccc} \text{Author:} & \text{Bas ten Haaf} \\ \text{Student ID:} & 1606034 \\ \text{Supervisor:} & \text{Daniela Kraft \& Melissa Rinaldin} \\ 2^{nd} \text{ corrector:} & \text{Thomas Schmidt} \end{array}$

Leiden, The Netherlands, June 18, 2017

The effect of curvature on diffusion in solid supported lipid bilayers

Bas ten Haaf

Huygens-Kamerlingh Onnes Laboratory, Leiden University P.O. Box 9500, 2300 RA Leiden, The Netherlands

June 18, 2017

Abstract

Theoretical models have shown that the geometry of cell membranes affects the diffusion rate of both proteins and lipids in the cell membrane. In this thesis we present a setup that has been developed to study two different diffusion effects. The first is the effect of curvature on a field of lipids and the second is the effect of curvature on diffusing colloidal particles. The setup consists of microsized 3D printed structures characterized by different curvatures combined with colloidal particles DNA linked to the structures. Quantitative data has been collected on the motion of the lipids in spherically curved bilayers on the structures, as well as qualitative data on the mobility of different colloids. The setup has been developed to the point that it can soon be used for collecting quantitative data on the colloidal motion.

Keywords: Solid supported lipid bilayer, curvature influenced diffusion, membrane protein, colloidal particles.

Contents

In	trodu	ction		1
1	The	oretical back	ground	5
	1.1		~	5
		1.1.1 Diffu	ision on a sphere	6
	1.2	On modelin	g the cell membrane	7
			supported lipid bilayers	7
		1.2.2 Colle	oidal particles	8
	1.3	Fluorescenc	e microscopy	9
		1.3.1 Fluo	rescence recovery after photobleaching	11
2	Met	hodology		13
	2.1	Materials		13
	2.2	Experiment	al set-up	14
	2.3	Set-up prep	aration	15
		2.3.1 SUV	formation	15
		2.3.2 Collo	oid treatment and coating	16
		2.3.3 Subs	trate treatment and coating	16
		2.3.4 Link	ing colloids to a SLB	16
		2.3.5 Desi	gn and development of microstructures	17
			a coating polystyrene particles	18
	2.4	Imaging and	d analysis	19
3	Res	ults		21
	3.1	Part 1: Diffu	sion of a field of lipids	21
		3.1.1 Colle	ected data	23
	3.2	Part 2: Collo	oid mobility	31

vi		CONTENTS
4	Conclusion	35
5	Acknowledgments	37

Introduction

All known life on earth shares the common feature of being made up of different cells that work together to form structures and regulate all the required life processes. In order to improve our comprehension of life at a larger scale, we first need to come to understand the rules that govern single cell behavior.

An important structure present in all cells is the plasma membrane, a thin bilayer of amphiphilic lipids that separates the inside and the outside of the cell. A large collection of membrane proteins resides within the layer of lipids. They carry out essential tasks such as movement of nutrients, cell signaling and fixating the cell in certain locations[1].

Membrane protein move throughout the lipid membrane by diffusion, as described by the 'fluid mosaic model' proposed by S.J. Singer and G.L. Nicholson in 1972 [2] (see Figure 1). In this model, cell membrane curvature is seen as a passive result of cell activity and proteins are free to move laterally in the membrane. The lipids making up the membrane freely move around as well. Theoretically this would result in a random distribution of protein throughout the membrane. On the contrary, experimental results show that protein are not randomly distributed and protein movement is in many cases slower or even confined to specific locations.

In systems such as neural networks it has been shown that voltage-gated ion channels have to be at the right place in the right number to give the neuron its specific characteristics. Improper or random ion channel localization in this system would cause communication defects in the neural network[4].

These results have led to the idea that membrane curvature is not a passive feature, but rather the result of protein and lipid interactions that dynamically transform the cell membrane[5, 6], which in turn leads to protein movement to specific sites. This is called protein targetting. Membrane

2 CONTENTS

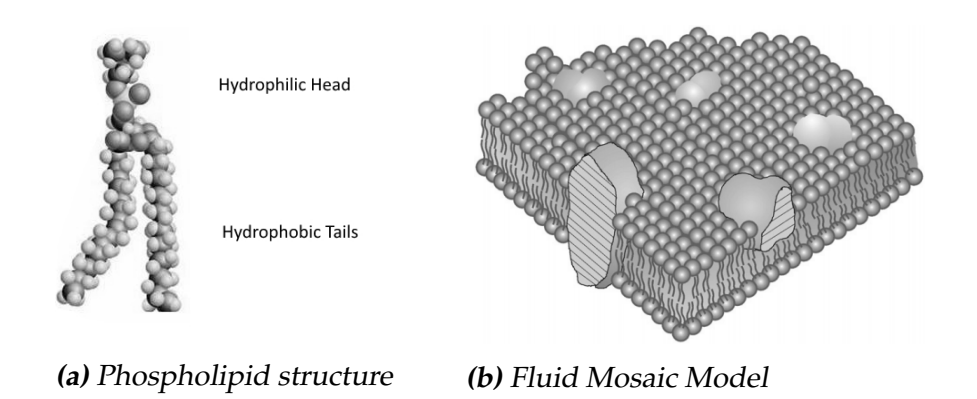


Figure 1: a) The phospholipid structure, consisting of a hydrophilic (water loving) head and a hydrophobic (water hating) tail. b) Representation of the fluid mosaic model as originally proposed. The phospholipids self assemble in a bilayer due to their amphiphilic nature. Protein can be seen embedded in the bilayer with two types of membrane protein displayed, one embedded in the bilayer and the second through the membrane.[3]

shaping protein have been identified and malfunctioning of these protein has been shown to be the cause of certain human disease[7, 8] due to needed protein no longer moving to the right site.

A proposed cause for the protein targeting effect is that the local curvature of membranes influences the diffusion of protein.

The hypothesis has led to the study of two different topics:

1. The effect of surface membrane protein on membrane curvature. An example of protein induced membrane curvature has been identified by Prevost et al. [9].

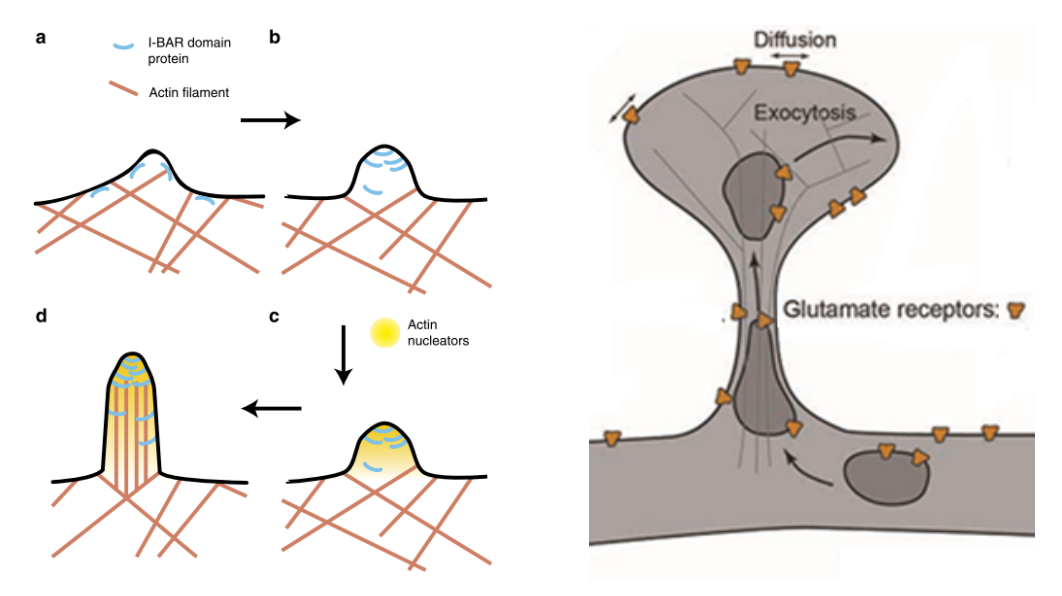
2. The influence of membrane curvature on protein movement. Protein in specific biological structures such as dendritic spines in the neural system were shown to have their motion strongly affected by the geometrical properties of the structures [11].

Both these effects are displayed in Figure 2.

We are interested in looking further into the second topic, aiming to look at diffusion of the field of lipids in the membrane as well as the particles in the membrane. Experimental study on the isolated effect of curvature on diffusion has shown that the curvature of the cell membrane does indeed influence protein targeting[12], but the effect has not been quantified. This is largely due to the difficulty with actively controlling cell membrane curvature and observing protein.

In this thesis we present an artificial cell membrane model consisting of

CONTENTS 3



- (a) Membrane curvature due to protein interaction
- **(b)** Dendritic spine with receptor protein

Figure 2: a) Diagram displaying how the presence of i-BAR domain protein in the membrane can lead to cell membrane deformation [9]. b) Diffusion of receptor protein in dendritic spine has been shown to be strongly affected by the geometrical properties of the spines [10][11].

colloidal particles DNA linked to a polymer supported lipid bilayer on a substrate with known, fixed geometry.

The setup has been developed to the point where we achieved data collection on the diffusion rate of lipids in the curved bilayer using fluorescence recovery after photobleaching techniques. Furthermore we are very close to having the DNA linked colloid system functional and we present our progress in this area.

In the first chapter of this thesis we discuss the theoretical background in support of our experiment and in the second chapter we detail the materials and methods we have used. In the third chapter we present the results achieved by our investigation and in the fourth chapter we outline the conclusions that we can draw from these results.



Theoretical background

1.1 Brownian motion

Micrometer sized particles in solution are in a constant random motion called Brownian motion. The effect, first studied by Robbert Brown, is the result of constant collisions between the particles and the molecules in the solution from every direction that leads to a net overall force in a random direction. By looking at this concept from a statistical viewpoint, Einstein quantified the diffusion of an ensemble of particles and derived the equation for the mean square displacement of these particles as a function of time [13]. By showing that the particles per unit volume C(x,t) for N particles undergoing Brownian motion in one dimension satisfies the diffusion equation:

$$\frac{\partial C}{\partial t} = D \frac{\partial^2 C}{\partial x^2} \tag{1.1}$$

it is possible to derive the probability density distribution at position x at a certain time t:

$$C(x,t) = \frac{N}{\sqrt{4\pi Dt}} e^{-\frac{x^2}{4Dt}}$$
 (1.2)

This distribution is a normal distribution with $\mu = 0$ and $\sigma^2 = 2Dt$ and leads to the following relation between the diffusion coefficient D and the root mean square displacement x_{RMS} for a single particle:

$$x_{RMS} = 2Dt (1.3)$$

This result for one dimension can be extended to n dimensions, using the following equation:

$$x_{RMS} = 2nDt (1.4)$$

Although our understanding of these equations for diffusion in three dimensions or for diffusion confined to a flat two dimensional system is complete, the knowledge of diffusion of particles confined to two dimensional surfaces of arbitrary shape is still lacking.

In this thesis we will focus on spherical surfaces, due to the symmetries associated with spheres that simplify the problem. The theory for Brownian motion on a spherical surface is presented below.

1.1.1 Diffusion on a sphere

The theory presented below is relevant for a field of particles with a size much smaller than the spherical surface, so that we can apply it to model the behavior of the field of lipids on a curved spherical substrate.

When investigating motion on a spherical surface, it is convenient to introduce spherical coordinates: $x = r\cos(\theta)\sin(\phi)$, $y = r\sin(\theta)\sin(\phi)$, $z = r\cos(\phi)$. The diffusion equation in spherical coordinates for a field of particles C is written as:

$$\frac{\partial C}{\partial t} = \frac{D}{r^2} \frac{\partial}{\partial r} (r^2 \frac{\partial C}{\partial r}) + \frac{D}{R^2 \sin(\theta)} \frac{\partial}{\partial \theta} (\sin(\theta) \frac{\partial C}{\partial \theta}) + \frac{D}{R^2 \sin^2(\theta)} \frac{\partial^2 C}{\partial \phi^2}$$
(1.5)

Now since the problem is confined to a spherical surface of constant r=R, radial symmetry can be applied. Furthermore we consider a particle that starts moving from the top of the sphere, so that we can apply symmetry in the ϕ coordinate. Under these assumptions the radial and ϕ terms drop out of the diffusion equation so that it becomes:

$$\frac{\partial C}{\partial t} = \frac{D}{R^2 \sin(\theta)} \frac{\partial}{\partial \theta} (\sin(\theta) \frac{\partial C}{\partial \theta})$$
 (1.6)

As with *Equation 1.3*, the solutions of *Equation 1.6* can be calculated analytically and the root mean square displacement can be derived. This has been done by Paquay et al.[14], who found the following result for the root mean square displacement of particles confined to a spherical surface:

$$x_{RMS} = 2R^2(1 - e^{-\frac{2Dt}{R^2}}) {(1.7)}$$

This result already provides some indication that the motion of the lipid field is affected by the curvature of the spherical surface, which is given by $\frac{1}{R^2}$.

It is noteworthy to mention that for $t \to 0$ we can expand $e^{-\frac{2Dt}{R^2}}$ to be

 $1 - \frac{2Dt}{R^2}$, so that we find $x_{RMS} = 4Dt$. This is the same as the result for a flat surface (*Equation 1.4*). Paquay et al. justify this by saying "for short times, the particles do not "feel" the geometric confinement, and the mean square displacement is just 4Dt, like in a 2D plane." We use the result by Paquay et al. in chapter 3 to derive an expression for the effective diffusion coefficient of a field of particles on a sphere.

1.2 On modeling the cell membrane

In this section a simple artificial system is introduced that can be used to study the diffusion of lipids and model the diffusion of proteins confined to a membrane. The model consists of a system of colloidal particles suspended on a solid supported bilayer. These two concepts are explained in the following two sections.

1.2.1 Solid supported lipid bilayers

A common method for modeling the cell membrane properties is through the use of solid supported lipid bilayers (SLBs), a lipid bilayer on a solid substrate. This model is used, because the geometry of the substrate can be set so that the curvature of the bilayer can be controlled.

The first step in SLB formation is the creation of small unilamellar vesicles (SUVs). SUVs are nanosized spherical lipid structures consisting of a

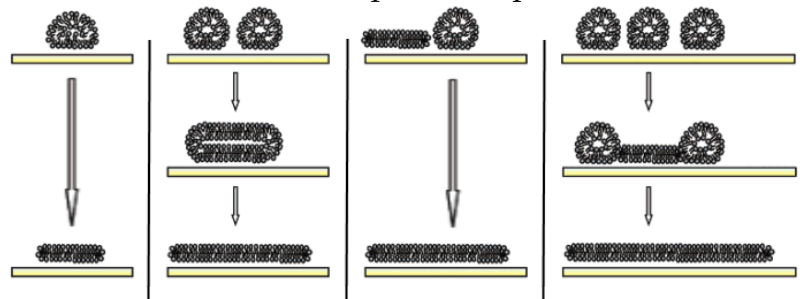


Figure 1.1: Schematic representation of different ways through which vesicle rupture can lead to bilayer formation [15].

single lipid bilayer. Vesicles form spontaneously in aqueous solution due to interplay between thermodynamics, interaction forces, and molecular geometry [16]. When these vesicles come into contact with a substrate they rupture onto the substrate and form a bilayer. This can occur spontaneously depending on a balance between the gain in adhesion energy and the cost in the vesicles curvature energy. Different ways in which vesicle

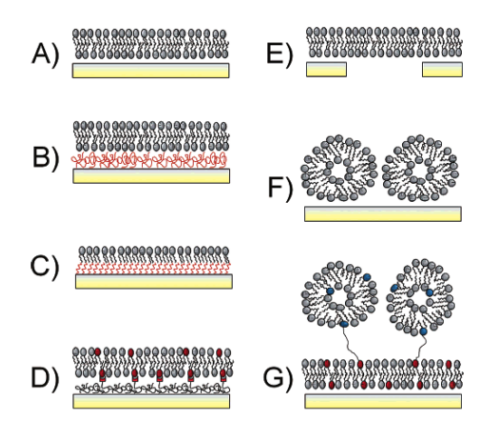


Figure 1.2: Diagram showing different SLB models. A) shows a normal SLB, B) and C) show a polymer cushioned bilayer, D) shows a tethered bilayer, E) shows a freely suspended bilayer and F) and G) show vesicular layers [15]

rupture can occur are displayed in *Figure 1.1*. Once the vesicles have ruptured to form a bilayer it is crucial that the lipids within the bilayer remain mobile to preserve the physical properties in of the bilayer.

The most important factors determining the success of forming a mobile SLB have been found to be the charge of the substrate, the presence of chlorine and the presence of silica in the substrate, where the presence of silica has appeared to be of greatest importance [15]. Recent work by Brouwer et al. however has shown that polystyrene particles, where silica is not present, can also be coated with a mobile bilayer [17]. SLBs come in a multitude of forms as

displayed in *Figure 1.2*, as polymers can be added to cushion or tether the bilayer, which may influence the overall mobility [15].

1.2.2 Colloidal particles

The class of materials that lies between systems that are dispersed in bulk and systems that are dispersed molecularly is known as colloids. They are small particles with a size ranging from 1 to 1000 nanometers. An example of such a system is silica particles dispersed in an aqueous medium. Colloidal particles experience Brownian motion as described in *section 1.1*, due to interaction with the molecules in the solution.

One of the largest challenges in working with colloids is trying to maintain their stability. A colloidal dispersion is in a state of higher free energy than the material in bulk. It tends to pass to the bulk state spontaneously and is therefore unstable. Only if an energy barrier is present preventing this from happening will the colloidal particles remain meta-stable for sufficient time. The energy to carry a system over the energy barrier comes from the Brownian motion of the particles and their thermal energy [18].

Gravitational height of colloid particles

Due to the scales concerning colloids, gravitational effects may lead to sedimentation as the gravitational force is higher than the force created by

collision with molecules in the solution. When studying colloids to model protein, sedimentation is an unwanted effect as it is required that the colloids are able to move up and down without the influence of gravity. Due to thermal fluctuations this is possible to an extent.

The height a colloidal particle can reach due to thermal fluctuation against gravity is known as the gravitational height and given by:

$$h = \frac{k_b T}{F_g} \tag{1.8}$$

Where F_g , the gravitational force, is given by:

$$F_g = \frac{4}{3}\pi a^3 \Delta \rho g \tag{1.9}$$

with $\Delta \rho$ denoting the density mismatch between the colloids and the solvent in which they are dispersed, a denoting the radius of the colloid and g denoting the gravitational constant.

From Equation 1.8 and Equation 1.9 it is clear that the gravitational height can be raised by decreasing the radius of the particles, increasing the temperature or reducing the density mismatch[19].

1.3 Fluorescence microscopy

Fluorescence microscopy is a microscopy technique that makes use of fluorophores; substances that absorb light and re-emit it at a different wavelength. This occurs due to the excitation and relaxation of molecules within the substance.

The technique uses the aforementioned shift in wavelength, called the Stokes shift, by exciting fluorophores and then completely filtering out the excitation spectrum, allowing only the resulting emitted spectrum through. An illustration of these spectra can be seen in *Figure 1.3*.

This method allows objects that fluoresce to be observed, mostly filtering out anything that does not. Labeling certain biological object with fluorophores allows trajectories of particles to be followed or the concentration of substances to be studied, making fluorescent microscopy a very popular imaging method in biology. Using fluorophores with different emission spectra allows simultaneous imaging of many different structures[20, 21]. The simplest fluorescence microscopy set-up uses so called epi-illumination. In this set-up a dichroic mirror is used to separate the emission from the excitation light (displayed in *Figure 1.4a*) and a series of filters ensures that only the right wavelengths reach the sample. To

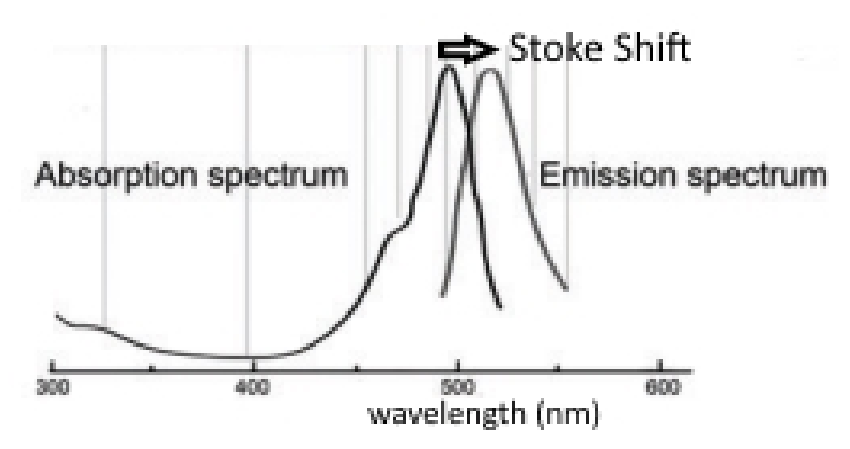
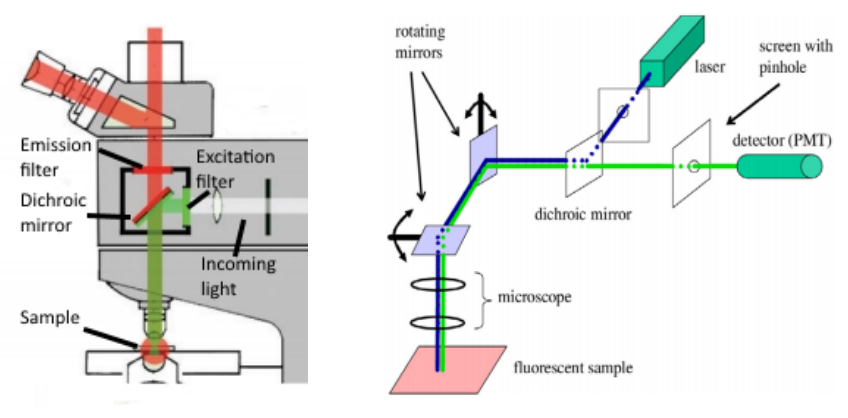


Figure 1.3: An example of an absorption and emission spectrum. The difference between the two peaks of the spectra is known as the Stoke shift, the effect that allows fluorescence microscopy to work [20].

improve the acquired image in fluorescence microscopy a small change is made to the epi-illumination setup in confocal laser scanning microscopy (CLSM), displayed in *Figure 1.4b*. In CLSM a screen with a small pinhole is placed at the focal point of the emission laser and the excitation light, to filter out any light that is out of focus. Between the sample and the dichroic mirror two rotating mirrors are added that turn quickly to scan the sample with the laser. This allows for quick video imaging of a fluorescent sample.



(a) Epi-illlumination microscopy

(b) Confocal Laser Scanning Microscopy

Figure 1.4: A)Diagram displaying epi-illumination microscopy[20] B) Diagram displaying Confocal Laser Scanning Microscopy [19].

1.3.1 Fluorescence recovery after photobleaching

A fluorophore molecule that shows fluorescence is excited to a high energy state and subsequently decays to its ground state, emitting a photon. This cycle can in principle repeat forever, however the circumstances in which fluorophores are used in microscopy usually result in a limit of about 10.000 to 40.000 cycles before the fluorophores experience a permanent loss of fluorescing ability. The loss of fluorescing ability is known as bleaching.

A proposed mechanism to explain bleaching is that an excited fluorophore in its triplet state can interact with an oxygen molecule to excite it to its singlet state. Singlet state oxygen is very reactive and may engage in chemical reactions with the fluorophore, altering its chemical composition[20].

In general bleaching is an unwanted phenomenon that leads to loss of signal over time, nevertheless it also has applications. Bleaching is a very useful tool in a technique that determines mobility of fluorophores called Fluorescence Recovery After Photobleaching (FRAP).

In FRAP a small region of the sample is illuminated with a very high intensity laser, causing all the fluorophores in the region to bleach. By diffusion of outside fluorescent molecules into the region, fluorescense in the area is recovered. A typical FRAP curve is detailed in *Figure 1.5*.

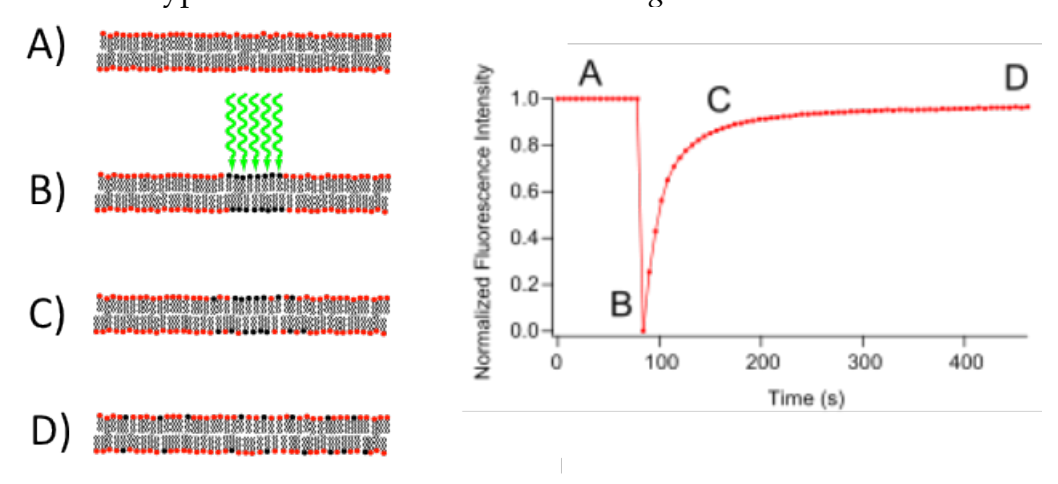


Figure 1.5: Graphical representation of FRAP and the expected corresponding graph of fluorescence intensity recovery over time in the area. A) Sample before bleaching B) Bleaching has occurred resulting in loss of fluorescence C) Recovery of fluorescence as fluorescent molecules diffuse D) Full recovery [22].

On analysis of the recovery curve

The derivation of the diffusion coefficient from the recovery curve for FRAP on a flat surface has been developed by Axelrod et al.[23]. The technique uses an intensity profile I(r) that describes the bleaching laser intensity at a certain place r and the solution for the particles per volume C(r,t) at place r and time t of the diffusion equation. The solution is calculated using an initial condition dependent on the intensity profile:

$$C(r,0) = C_0 e^{-\alpha T I(r)},$$
 (1.10)

where T is the duration of bleaching. The fluorescence F(t) that will be observed at a time t after bleaching is then defined as an integral over the bleached area:

$$F(t) = \frac{q}{A} \int I(r)C(r,t)d^2r$$
 (1.11)

where q and A are constants related to quantum effects of the laser. Axelrod et al. calculate the recovery curve for a Gaussian intensity profile and find the following relation between the diffusion coefficient and the time-characteristic of the recovery curve:

$$D = 0.25 \frac{w^2}{t_{\frac{1}{2}}} \tag{1.12}$$

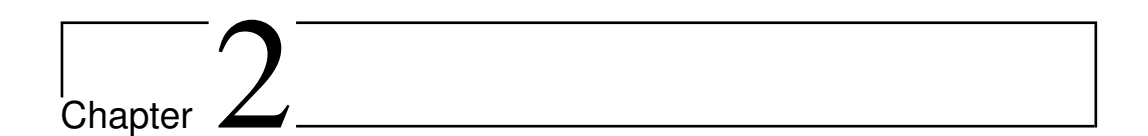
where w represents the radius of the beam and $t_{\frac{1}{2}}$ represents the time it takes to recover half of the maximum fluorescence.

In practice multiple ways are used to retrieve an accurate value for the recovery halftime $t_{\frac{1}{2}}$. A commonly used method is to use the recovery curve derived by Axelrod et al. (*Equation 1.13*) to fit the data.

$$F(t) = \frac{q}{A} \sum_{n=1}^{\infty} \frac{(-K^n)}{(n+1)!} \frac{1}{1 + \frac{2t}{\tau_{\frac{1}{2}}}}$$
(1.13)

In recent years however, easier alternatives have been developed. One alternative has been developed that uses exponential fitting, derived from modeling the recovery as a chemical reaction [24]. Exponential fitting of FRAP data has been used in our group in 2015 by Vegter et al. and was found to be a valid approach[25]. We further discuss the fitting procedure in *section* 2.4.

The above method for determining the diffusion coefficient can in principle be extended to curved surfaces. To do this the intensity profile and the solution to the diffusion equation are required.



Methodology

2.1 Materials

The table below lists the materials used in the investigation (*Table 2.1*). *Table 2.1: Materials*

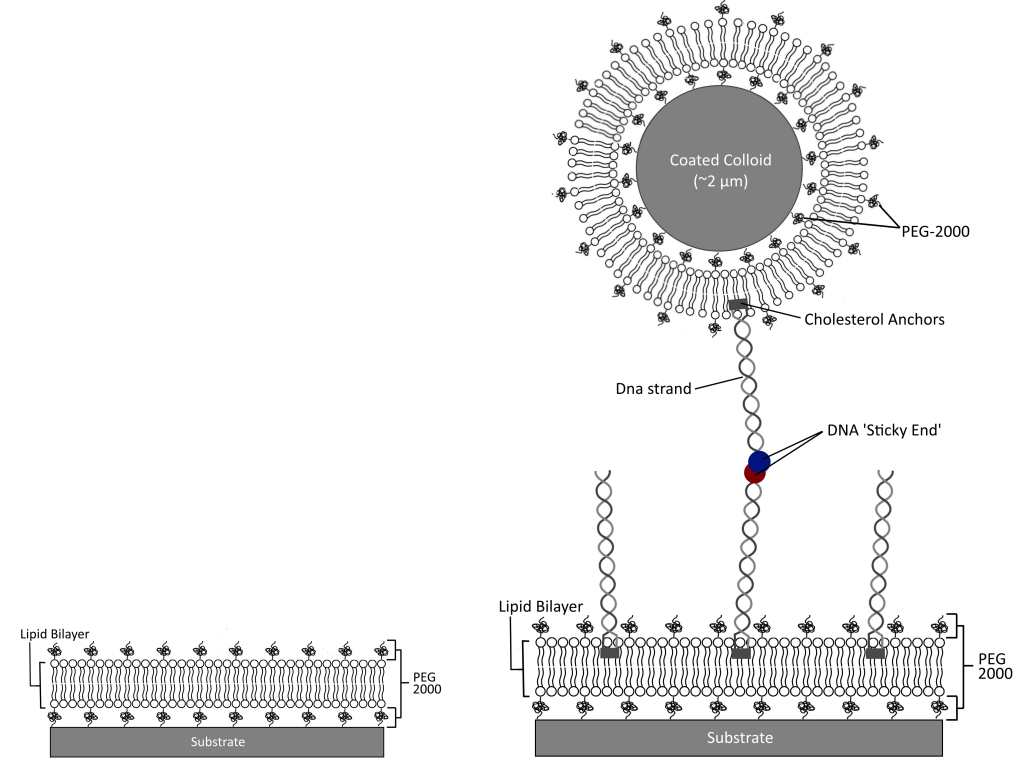
	Description	Short Name
Phospholipids	1,2-dioleoyl-sn-glycero-3-	DOPC
Thospholipius	phosphocholine	DOIC
	1,2-dioleoyl-sn-glycero-3-	
	phosphoethanolamine-N-	DOPE-PEG2000
	[methoxy(polyethyleneglycol)-2000]	
	1,2-dioleoyl-sn-glycero-3-	
	phosphoethanolamine-N-	DOPE-Rhod
	(lissaminerhodamine B	DOI E-MIOU
	sulfonyl)	
Solvent	4-(2-hydroxethyl)-1-	HEPES
Solvent	piperazineethanesulfonicacid	TILILO
Substrates	Organically modified ceramic	ORMOCER
	Circular D 263 M Colorless	
	borosilicate Glass	Glass Coverslip
	coverslips.Thickness: 0.16 - 0.19mm	Glass Coversilp
	Diameter: 25mm	
Cleaning-	Milli-Q-water	MQ
solutions	Ethanol	EtoH
	Hellmanex III	Hellmanex

In addition $0.9 - 2\mu m$ silica and polystyrene spheres are used as colloids.

14 Methodology

2.2 Experimental set-up

The experimental set-up developed for the project is detailed in the figure below (*Figure 2.1*). Using this setup two different effects can be studied. The setup shown in *Figure 2.1a* is developed for studying the motion of lipids within the bilayer. The geometrical properties of the substrate can be controlled. The setup is extended to the setup shown in *Figure 2.1b*, which we can use to study the effect confinement to a curved substrate has on colloids.



(a) Setup for investigating lipid motion

(b) Setup for investigating colloidal motion

Figure 2.1: Representation of the experimental setup developed for the investigations. Setup a) shows a substrate coated with a polymer (PEG_{2000}) cushioned SLB, which can be used to study the motion of lipids. Using setup a) we can prepare setup b), by addition of a SLB coated colloid. To the substrate and the colloid strands of DNA are then added with different open end sequences, as described in subsection 2.3.4. These sequences are complimentary and able to bind each other strongly. This link limits the particle to 2D movement on the substrate.

2.3 Set-up preparation

2.3.1 SUV formation

The spherical structures formed spontaneously by lipids in aqueous solution, called liposomes, come in a multitude of forms, classified by the number of bilayers [26]. The smallest of these liposomes are the SUVs needed for SLB formation. In order to create a solid supported bilayer of only one layer thin, it is crucial to prepare an even SUV solution without any larger structures. When the lipids are deployed in aqueous solution, a mix of SUVs and larger structures will be formed. There are multiple ways of filtering the mixture to only contain SUVs.

In our experiment we use the technique described by Stef van der Meulen [27], where extrusion is used to create SUVs. DOPC en DOPE-PEG₂₀₀₀ are mixed in a 40:1 molar ratio in chloroform. $1\mu l$ of DOPE-PEG₂₀₀₀-Rhodamin can be added as a fluorophore for allowing observation of the sample under a fluorescence microscope. The solution is left in vaccuum for 2 hours to evaporate the chloroform, after which the solution is rehydrated with HEPES to create a 2g/l solution. The mixture is then extruded 21 times. In extrusion the lipid solution is repeatedly forced through two Avanti polycarbonate filters with 30nm pores until only SUVs are left in the solution. The extrusion process is described in the online Avanti Extrusion Guide. Resulting SUVs are stored at 4 degrees and generally stable for around 4 days, higher temperatures or freezing will reduce this lifetime [28].

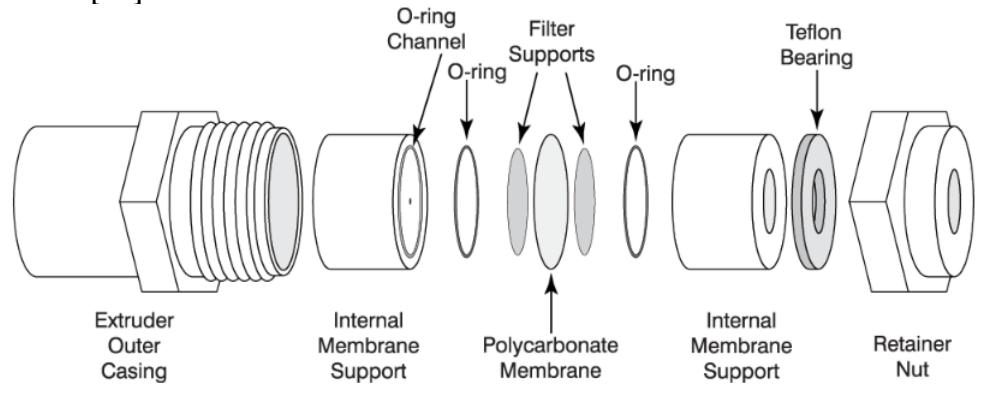


Figure 2.2: Exploded diagram detailing the setup used for extrusion [28].

16 Methodology

2.3.2 Colloid treatment and coating

The colloids we use in the experiment differ for size and material. We use $2.06\mu m$ and $0.906\mu m$ silica, $0.93\mu m$ polystyrene and $1\mu m$ silica coated polystyrene particles. The process through which silica particles are coated with polystyrene is described in *subsection* 2.3.6.

Colloids in salt solution will not be stable for a long amount of time as they will start to aggregate (1.2.2). Aggregation of the colloids is prevented by storage in milicule water or ethanol. Colloidal clusters in the solution are separated by alternately sonicating and vortexing the solution.

Before each use the colloids are washed with MQ water by centrifuging for 15 minutes at 3000 rpm.

To coat colloids we mixed $15\mu l$ of stock solution with $600~\mu l$ of HEPES and $50~\mu l$ of SUVs. The HEPES contains NaCl solution, as the presence of chlorine promotes SLB formation

The solution is then left to slowly rotate for 1 hour at 10 rpm to allow homogeneous bilayer coating on the particles. Without homogeneous coating empty patches on the particles will cause particles to stick to the substrate. Next the particle-SUV solution is washed again for 15 minutes at 3000 RPM to remove access SUVs.

2.3.3 Substrate treatment and coating

As substrate we use 30mm glass cover slips coated with 3D-printed microstructures. In order to clean the substrate and ensure an SLB can form the cover slips are submerged under gentle stirring for 30 minutes in Hellmanex, 30 minutes in Ethanol and 30 minutes with MQ water. The cover slips are rinsed in MQ water 3 times in between adding each solution. To coat the cover slips $600~\mu l$ is added to the cover slip together with $40\mu l$ of SUVs. The mixture is allowed to settle for an hour to allow an SLB to form. Afterwards the cover slip is washed to get rid of excess SUVs by removing solution from the cover slip and quickly adding new HEPES.

2.3.4 Linking colloids to a SLB

We use the technique described by Chakraborty et al. to link the colloids to the substrate, so that the colloids are confined to movement on the substrate [29]. Two different kinds of DNA linkers are added separately to the SLB coated colloid solution and to the SLB coated cover slip. The DNA linkers consist of a DNA strand with complimentary open ends that strongly bind together (*figure 2.3*).

In order to link the DNA we keep the colloids in rotation for 1 hour. At the same time we add the DNA to the bilayer. Afterwards they are both washed with HEPES to remove excess DNA. This is done in order to prevent DNA linkers from the cover slip solution to link the colloids, as this would cause the colloids to link together. It is important that the right

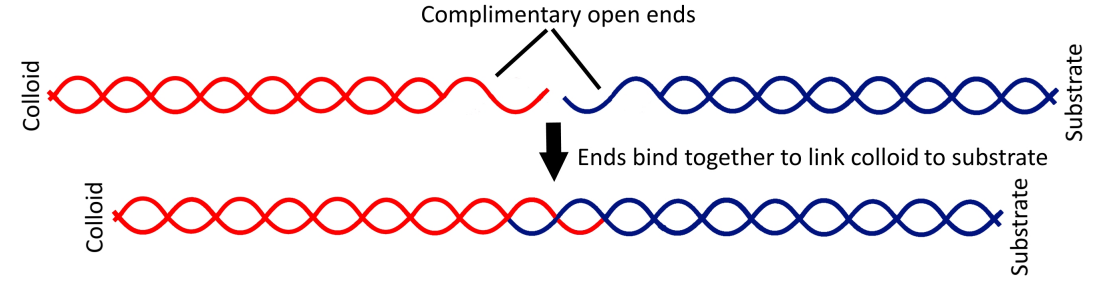


Figure 2.3: Schematic representation of DNA linking mechanism. concentration of DNA linkers is added to the solutions, as too large an amount would completely inhibit the motion of the colloids, while too little decreases the amount of colloids that are successfully linked. In the work by Stef van der Meulen on which our SUV preparation method is based a 2-5µl solution of cholesterol-conjugated DNA-linkers is used [27].

2.3.5 Design and development of microstructures

To create a curved substrate we use 3-D printed micro-structures with different geometries. Using a nanoscribe, structures with 200 nanometer resolution can be printed onto a glass cover slip. The structures are designed using 'Autodesk Inventor', a tool that allows for easy creation of 3-D objects from simple 2-D sketches. The material used by the nanoscribe has been shown in preliminary tests to be able to support a mobile supported lipid bilayer. The structures we have chosen to use in the experiment are displayed in *Figure 2.4*: hemispheres and inverted hemispheres of varying sizes. Spherical shapes were chosen on the basis of having a constant, radius dependent Gaussian curvature K and mean curvature K and mean curvature K and the effect of curvature can be easily studied by varying the radius of the spheres.

18 Methodology

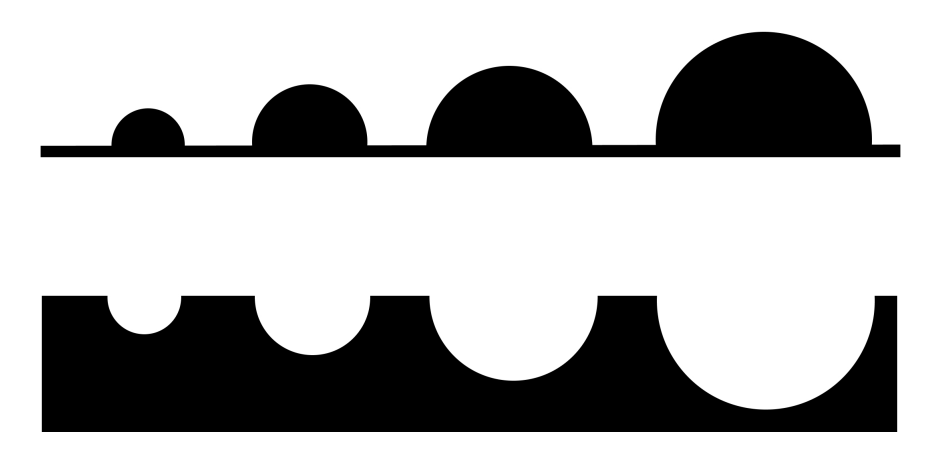


Figure 2.4: 2D representation of the two microstructures used in the experiment.

2.3.6 Silica coating polystyrene particles

As mentioned in *subsection* 1.2.1, the presence of silica strongly influences the chance of successful SLB formation. Polystyrene particles are much lighter than silica, but much harder to coat with a mobile SLB. It is therefore beneficial to coat polystyrene particles with a thin layer of silica.

To coat polystyrene particles with silica we use the Stober-growth technique described by Graf et al.[30], as displayed in *Figure 2.5*. The technique works for a range of materials. The procedure consists of two steps. PVP (poly(vinylpyrrolidone)) is added to polystyrene particles and allowed to adsorb. Particles are transferred to ethanol, where an ammonia solution is added (29.3 wt % in H₂O). Growth of the silica shell is then initiated by addition of Tetraethyl Orthosilicate (TEOS) under stirring at 600 rpm. Thickness of the shell is determined by total amount of added TEOS. For our experiment we skip the PVP step, as it is not required for silica particles.

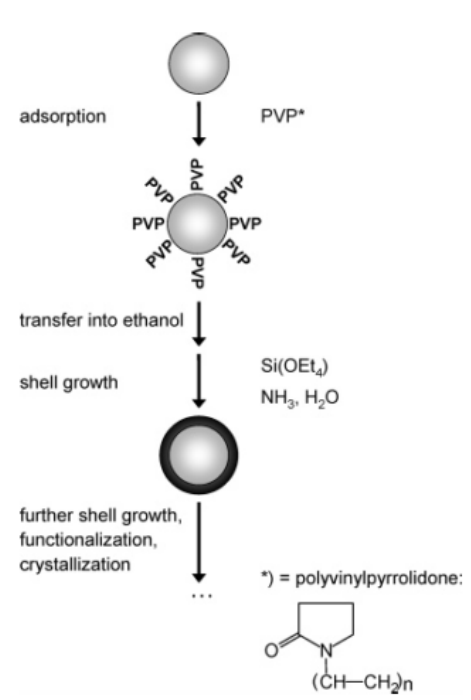


Figure 2.5: Schematic overview of silica coating process[30]

2.4 Imaging and analysis

Imaging of the set-up is done with the Nikon A1+ confocal microscope. Fluorescence recovery after photobleaching method is carried out in the microscopes Galvano mode with a 561nm wavelength for the red Rhodamine fluorophores that are present in our SLBs.

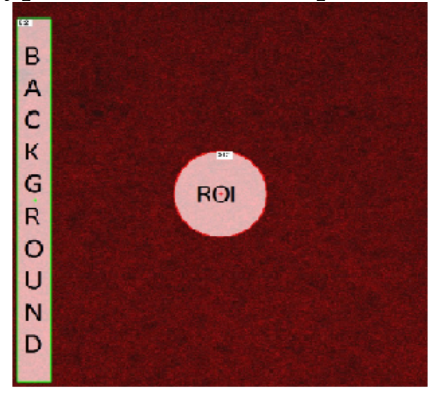
Normalization and fitting

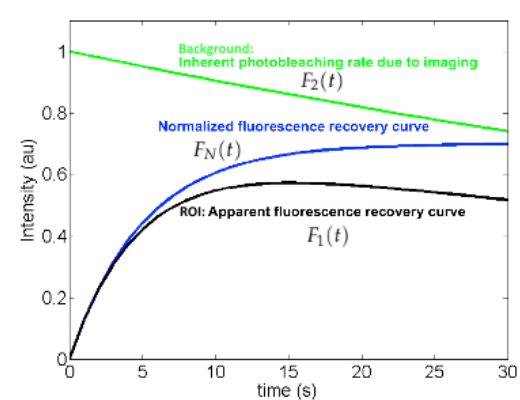
Since bleaching occurs continuously after the high intensity pulse, due to imaging, the recorded signal must be normalized in order to accurately analyze the date.

In order to do this the fluorescence in a large area near to the bleached area is observed simultaneously. Data from the bleached area $F_1(t)$ is then normalized by dividing by the data from the background area $F_2(t)$:

$$F_{Normalized}(t) = \frac{F_1(t)}{F_2(t)}$$
 (2.1)

Typical data for such a procedure can be seen in *Figure 2.6*. After normal-





(a) Measurement area selection

(b) Typical FRAP recovery curves

Figure 2.6: a) Image showing how the bleaching area is selected [31]. b) Graph showing typical curves for the background measurement, fluorescence recovery measurement (ROI) and the resulting normalized recovery curve $F_N(t)$.

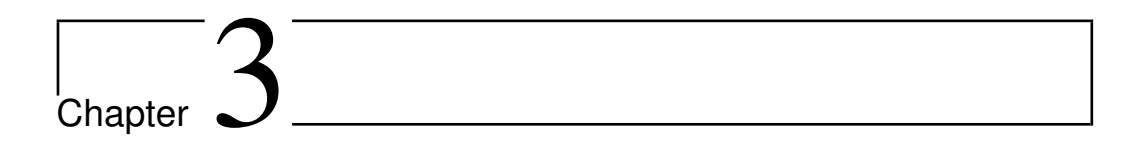
ization the resulting curve can be analyzed to obtain the half time of the recovery. The half time is required to determine the diffusion coefficient of the diffusing fluorescent particles, as described in *section 1.3.1*. The exponential fit we will use to recover the half time is:

$$F_N(t) = A(1 - e^{\frac{t}{\tau}}) + B \tag{2.2}$$

20 Methodology

where τ is the characteristic recovery time and A and B are parameters concerning the starting intensity and fraction of recovery. This method has been used previously by Salaris et al. and Vegter et al. in our group to analyse FRAP on flat surfaces[31][25].

As noted in *section 1.3.1*, this is not the expected curve predicted by the theory of Axelrod et al. [23], but rather a method that has been developed later that allows for easier curve fitting of FRAP data [24].



Results

Using the setup and techniques described in the previous chapters quantitative data has been collected on the mobility of lipids in solid supported bilayers on hemispheres of varying radii. The set-up has also been tested for mobility of the DNA-liked colloids, to provide a qualitative analysis of the circumstances under which the setup was functional. The results of these two investigations are presented below, summarized in two parts. Part 1 concerns the mobility of a field of lipids in the SLBs and part 2 concerns the mobility of colloidal particles.

3.1 Part 1: Diffusion of a field of lipids

In this section the collected results on the motion of lipids are shown. In addition two different theoretical approaches to model the expected behavior of the effect of curvature on the diffusing lipids are presented.

Predicting curvature effect: field theory

Using elements from field theory, Piermarco Fonda derived an expression for the expected diffusion equation on a general curved surface*. His work is presented here to provide a theoretical prediction for the effect of curvature on the diffusion of a field of lipids on a sphere.

Starting out from the expression for the total energy E of a lipid field on a fixed geometry, given in terms of an integral over the field ϕ describing

^{*}Unpublished work.

22 Results

the lipids and a potential $w(\phi)$, we have:

$$E = \int_{\Sigma} \frac{D}{2} |\nabla \phi|^2 + w(\phi) dA$$
 (3.1)

where the first term describes diffusion and the second a potential. In the case of our undisturbed membrane $w(\phi)$ is 0. The evolution of the field ϕ in time is described by the reaction-diffusion equation:

$$\frac{\partial \phi}{\partial t} = \frac{\delta E}{\delta \phi} \tag{3.2}$$

Given E as an integral in *Equation 3.1*, $\frac{\delta E}{\delta \phi}$ can be found using the Euler-Lagrange equation:

$$\frac{\delta E}{\delta \phi} = \frac{\partial L}{\partial \phi} - \nabla \cdot \frac{\partial L}{\partial \nabla \phi} \tag{3.3}$$

where in this case $L = \frac{D}{2} |\nabla \phi|^2$. Solving the equation yields:

$$\frac{\delta E}{\delta \phi} = -D\nabla_{\Sigma}^2 \phi \tag{3.4}$$

where ∇_{Σ}^2 is the Laplace-Beltrami operator, the Laplace operator defined on a two dimensional surface. Plugging this result into *Equation 3.1* gives:

$$\frac{\partial \phi}{\partial t} = D\nabla_{\Sigma}^2 \phi \tag{3.5}$$

A common technique to study equations in curved geometries is to expand the Laplace-Beltrami operator in terms that are invariant on the geometrical surface. The simplest of these are the mean curvature H and Gaussian curvature K. Expanding to first order gives:

$$\frac{\partial \phi}{\partial t} = D\nabla_{\Sigma}^2 \phi + D(\beta H^2 + \gamma K) \nabla_{\Sigma}^2 \phi \tag{3.6}$$

In our specific investigation on spherical surfaces of radius R, $H^2 = K = \frac{1}{R^2}$, so we introduce $\alpha = \beta + \gamma$. This leaves the following equation for diffusion on a spherical surface:

$$\frac{\partial \phi}{\partial t} = (D + \frac{\alpha}{R^2}) \nabla_{\Sigma}^2 \phi \tag{3.7}$$

Comparing this to the diffusion equation on a flat surface, we can see that the effective diffusion coefficient for motion of a field (in our case of lipids) on a sphere is expected to be:

$$D_s = D + \frac{\alpha}{R^2} \tag{3.8}$$

Predicting curvature effect: root mean square displacement

On top of the result derived by Piermarco, we found a different route derivation specifically on spherical surfaces that leads to the same expression for the effective diffusion equation for a field of lipids on a sphere. Starting from the root means square displacement of particles on a spherical surface found by Paquay et al. [14], we rewrite *Equation 1.7* to give an expression for the diffusion coefficient on a spherical surface:

$$D_s = -\frac{R^2}{2t} ln(1 - \frac{x_{RMS}}{2R^2}) \tag{3.9}$$

Since x_{RMS} is small for lipids (order of micrometers), we can insert the Taylor expansion of $\ln(1-x)$: $\ln(1-x) \approx -(x+\frac{x^2}{2}+\frac{x^3}{3}+...)$ into Equation 3.9. To the first order this becomes:

$$1^{st}Order: D_s = \frac{x_{RMS}}{4t} \tag{3.10}$$

This is the same as the result for the diffusion coefficient D_{flat} on a flat two dimensional surface, as shown in *Equation 1.4*. Now approximating to second order we find:

$$2^{nd}Order: D_s = \frac{x_{RMS}}{4t} + \frac{x_{RMS}^2}{16tR^2}$$
 (3.11)

If we now apply that in first order we found $D_s = \frac{x_{RMS}}{4t} = D_{flat}$, we can substitute D_{flat} into Equation 3.11. The same result as Equation 3.8 is found:

$$D_s = D_{flat} + \frac{\alpha}{R^2} \tag{3.12}$$

where we now see that $\alpha = D_{flat}^2 t$. Note that again for $t \to 0$ we find that the geometrical contribution drops to 0, leaving $D_s = D_{flat}$. This again implies that on short time scales the field of lipids doesn't "feel" the geometry, as discussed by Paquay et al [14].

In the following section we use this prediction, as derived in the two separate ways shown above, to fit our collected data.

3.1.1 Collected data

Data has been collected on the mobility of lipids on hemispherical structures in two different planes, resulting in two data sets. The first data set was collected on 5 different hemispheres with radii of 5, 7, 10, 14 and 20

24 Results

 μm . Imaging took place on the bottom plane of the sphere, where it was easier to get a good signal under the fluorescence microscope. Measurements were also done on a flat structure printed with the nanoscribe to determine D_{flat} , but no good data could be collected due to technical difficulties. The second data set was collected on 6 different sizes of hemispheres with radii of 5, 7, 10, 14, 18 and 20 μm on the top planes of the spheres, where the bleached area size could be determined more accurately but the signal was worse. We applied FRAP, as described in *subsection 1.3.1*, in a small circular region on each of the hemispheres. We aimed to apply FRAP on top of each sphere, so the bleached area could be determined more accurately and so that boundary effects would not come into play.

Data set 1

A confocal image showing the sample of hemispheres used for collecting our first data set is seen in *Figure 3.1*. As background we used a region on

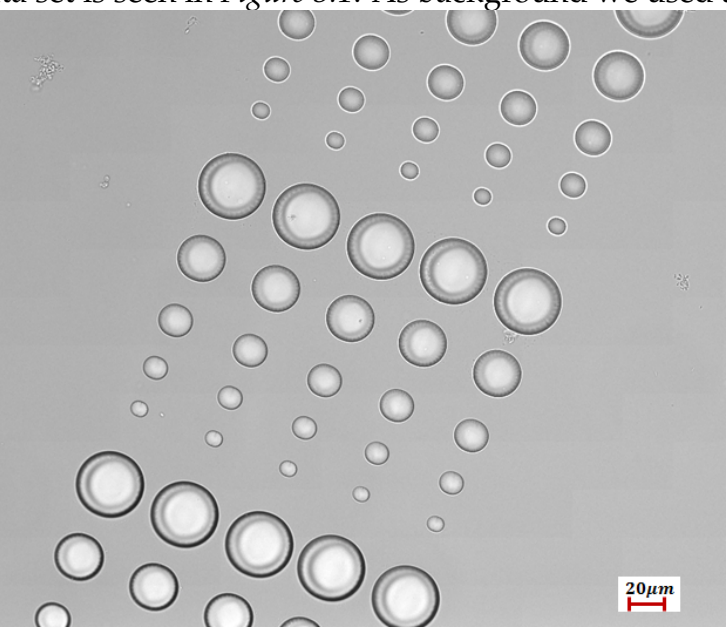


Figure 3.1: Confocal image of the bottom plane in which the first data set was collected.

a hemisphere that had not yet been bleached for FRAP. An example of this selection is seen in *Figure 3.2*. Once data was collected for FRAP on multiple hemispheres of each radius, the FRAP curves were fitted against the exponential fit described in *section 2.4*. From this fit the recovery halftime was determined and averaged for each hemisphere size. A table summarizing these results is seen below (*Table 3.1*).

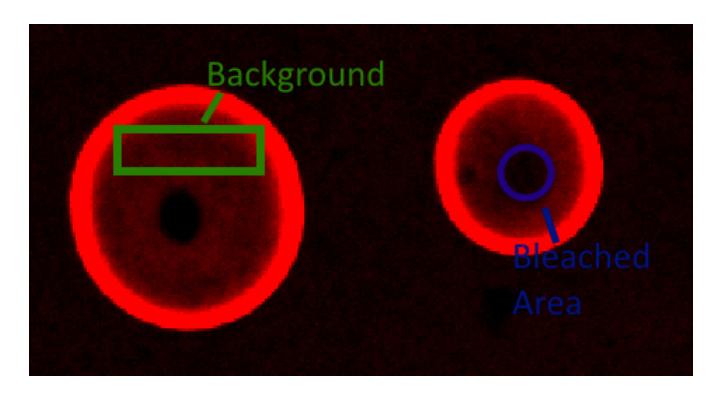


Figure 3.2: Fluorescence image of the setup in the bottom plane. The green rectangle shows the area used to measure the background. The blue circle shows the region selected for bleaching in the FRAP experiment. The background is used to normalize the FRAP data, as described in section 2.4.

Radius [µm]	5	7	10	14	20
# of measurements	1	5	5	4	4
Half time of recovery[s]	2.31	6.26 ± 1.04	10.14 ± 1.55	12.41 ± 1.66	13.41 ± 3.04
Bleaching region R [μ m]	1.16	2.92	2.92	2.92	2.92

Table 3.1: Table summarizing the collected data in the FRAPs on different sized hemispheres. The error in the halftime values were calculated using $\frac{\sigma}{\sqrt{N}}$. There is an unknown error in the halftime for smallest sphere, due to only 1 measurement being completed. Originally 5 measurements were done on the 14 and 20 μm hemispheres, however one datapoint had to be discarded for each hemisphere due to rapid bleaching occurring caused by poor microscope settings, which meant that the curves couldn't be properly analyzed.

The data from *Table 3.1* is represented graphically in *Figure 3.3*. As seen in this graph, we observed that the fluorescence recovery was faster for smaller spheres with higher curvature than for the larger spheres. Furthermore we saw that saturation takes place at larger radii, where the increase in recovery halftime decreases. This was to be expected, as increasing the radii further results in a surface that approaches a flat plane.

From the recovery half-times we calculated the diffusion coefficient of the lipids in the membrane. We did this using a simple estimation based on *Equation 1.12*. The top part in this equation represents the area of the bleached area on the flat plane πw^2 . To translate this equation to our curved surface, we replaced this area with the area bleached in our experiments. For a spherical cap of width ρ on a sphere of radius R, this area

26 Results

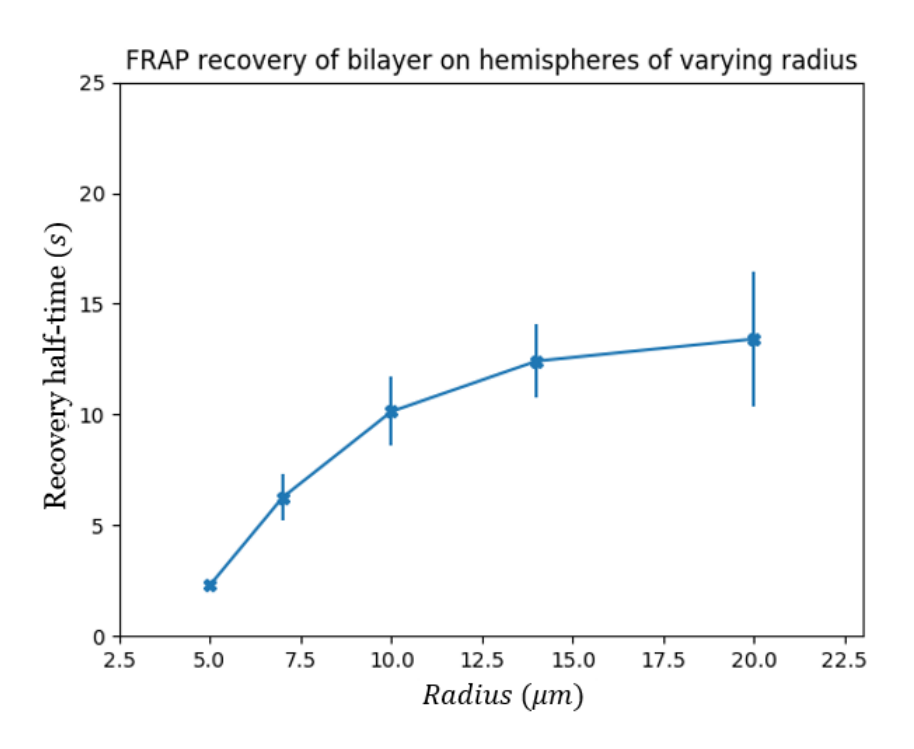


Figure 3.3: Graph of the halftime recovery of FRAP experiments for our hemispheres of different radii. Error bars are calculated as described under Table 3.1. The blue line connecting data points has been included to visualize the observed saturation of half time as the radius is increased.

is equal to $4\pi R^2(1-\sqrt{1-\frac{\rho^2}{R^2}})$. Changing *Equation 1.12* to be adjusted for our bleached area then gives the following estimate for the diffusion coefficient of the lipids in the bleached SLB:

$$D = \frac{4\pi R^2 (1 - \sqrt{1 - \frac{\rho^2}{R^2}})}{t_{\frac{1}{2}}}$$
 (3.13)

It should be noted that since this data set was imaged in the bottom plane, the actual bleached area could not accurately be determined, so that *Equation 3.13* is only an estimation. The halftime data from *Figure 3.3* was used to calculate the diffusion coefficient in the way described above, which resulted in the following graph for diffusion coefficient of the lipids against radius of the hemispheres (*Figure 3.4*).

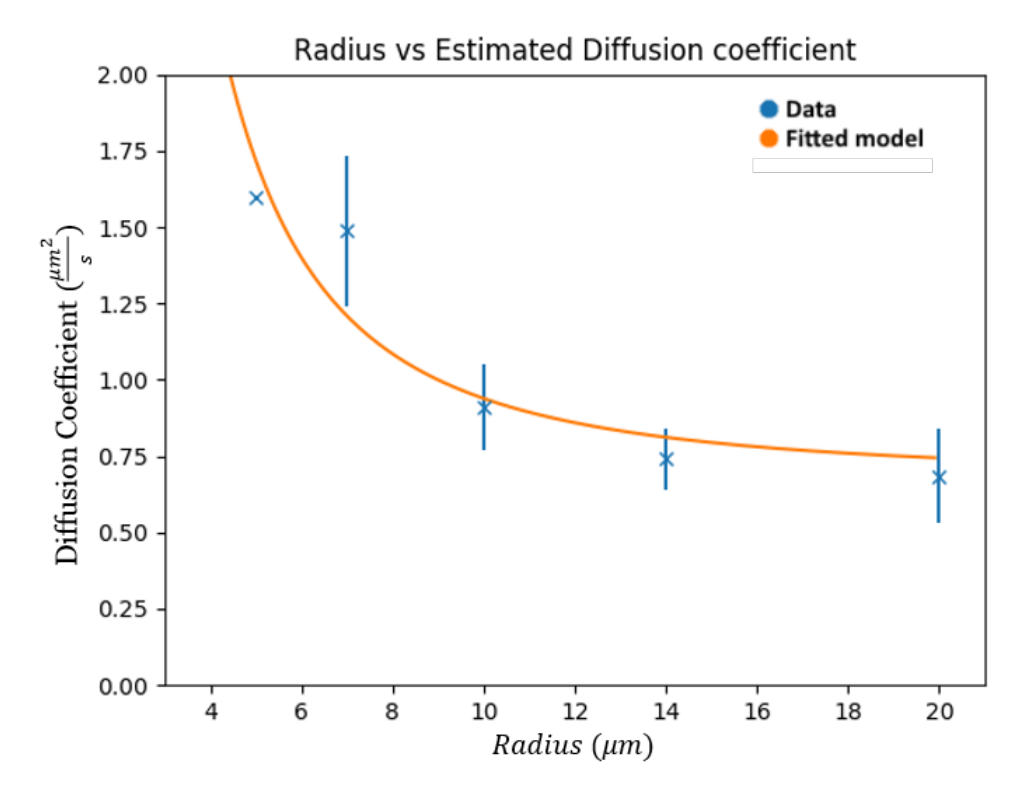


Figure 3.4: Estimated diffusion coefficient from the halftime data in Table 3.1. The fit shows the predicted trend $D_{flat} + \frac{\alpha}{R^2}$. The fit does not take in account the errors in the measurement, as we have an unknown error for the $5\mu m$ sphere. From this fit we find for this data a predicted value for D_{flat} of $0.68 \pm 0.12 \left[\frac{\mu m^2}{s}\right]$.

We fitted the graph of the lipids diffusion coefficient against hemisphere radius using $D_s = D_{flat} + \frac{\alpha}{R^2}$, as predicted in *section 3.1*. As can be seen in *Figure 3.4*, our data seems to agree reasonably with our predicted model. A value predicting D_{flat} could be obtained from the model and was found to be $0.67 \pm 0.12 \frac{\mu m^2}{s}$. Earlier work by Salaris et al. to directly determine the diffusion coefficient of lipids in an SLB on a flat glass coverslip found D_{flat} to be $0.7 \pm 0.21 \frac{\mu m^2}{s}$ [31].

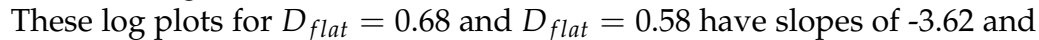
A common method to analyze the correctness of a predicted formula is by analyzing the slope of the log-log plot of the data. A log-log of our predicted relation $D_s = D_{flat} + \frac{\alpha}{R^2}$ would have a slope of -2 when plotting $log(D_s - D_{flat})$ against log(R):

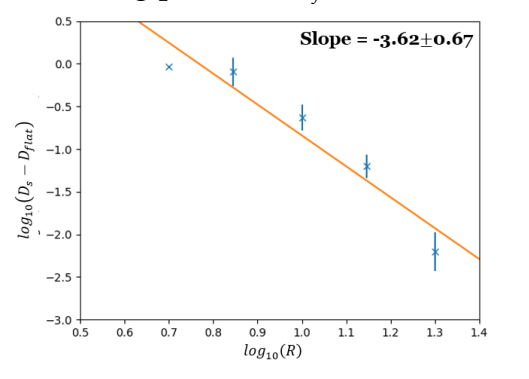
$$log(D_s - D_{flat}) = -2log(R) + log(\alpha)$$
(3.14)

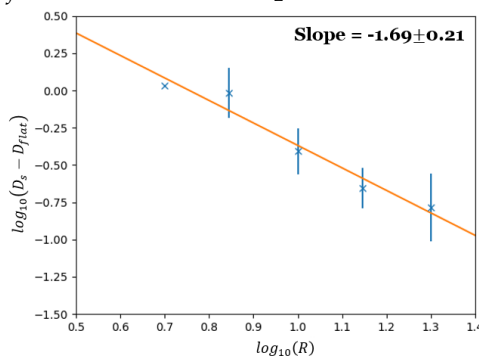
Since we don't know the actual value of D_{flat} for the material of our nanoscribe structures, we took the D_{flat} value taken from our model. We also used the lower bound of D_{flat} as provided by the error. The log-log plots

28 Results

are seen in Figure 3.5.







- (a) Log plot using $D_{flat} = 0.68$
- **(b)** Log plot using $D_{flat} = 0.56$

Figure 3.5: Two graphs where $log(D_s - D_{flat})$ are plotted against log(R) for two different values of D_{flat} . In graph a) the value of 0.68 is used, as retrieved from the model. In graph b) a value of 0.56 is used, which is the lower bound calculated for D_{flat} using the model. Slopes of -3.62 \pm 0.67 and -1.69 \pm 0.21 were found respectively.

-1.69 respectively. A very large variation in the slope appeared for minor variation in D_{flat} , so that we would like to highlight the importance of an accurate determination of D_{flat} .

Data set 2

For the second data set we repeated the FRAP measurements in the same way as conducted for the first data set, only now bleaching the hemispheres in the top plane. In addition we printed two extra hemispheres with radii of $18\mu m$ and $25\mu m$). The nanoscribe was unable to correctly print the $25\mu m$ hemispheres, so no data could be collected for this radius. Due to collecting data in the top plane of the spheres no other fluorescent bilayer was visible during the measurements besides the portion that we bleached. This made selecting a background more difficult. To get the best possible background we selected the entire visible region (including the region bleached for FRAP), which is valid under the assumption that the total amount of bleached and unbleached lipids within the region remains constant. The background selection is shown in *Figure 3.6*.

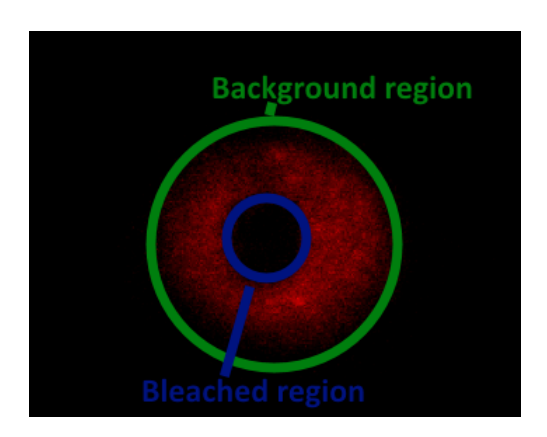


Figure 3.6: Image showing the choice of background and bleaching region for FRAP measurements on the top of the hemispheres. Image was taken right after the bleaching stage in FRAP

Imaging on top of the spheres in the fluorescent mode also required a much higher intensity, causing the entire bilayer to bleach much faster. This proved problematic, as the bleaching due to imaging occurred much faster than the recovery due to diffusion. This resulted in very steep or non-linear background curves, shown in *Figure 3.7*. Due to this problem,

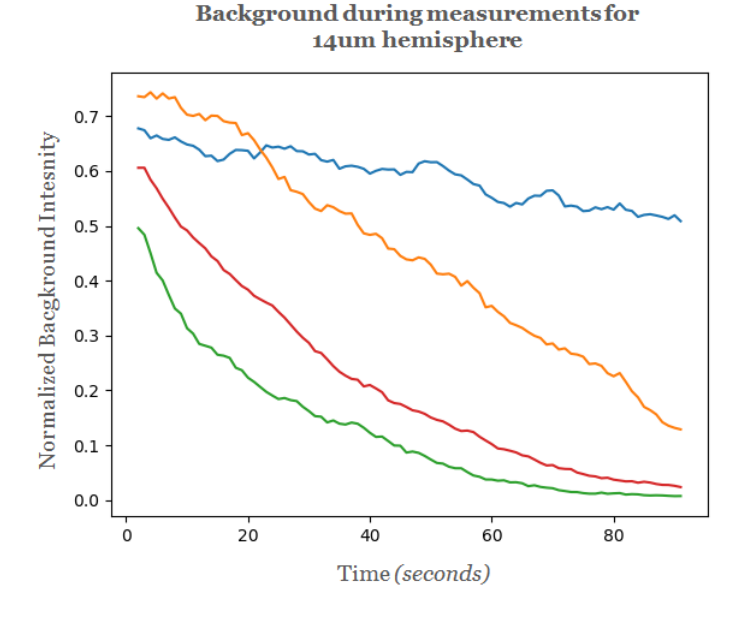


Figure 3.7: Example of four different background data recorded during four FRAPs on 14µm hemispheres. The background is seen to be very steep and nonlinear. The green line is an example of a measurement that had to be discarded due to poor, non-linear background data (before 55 seconds)

30 Results

normalizing the data by dividing it by the background data didn't give any useful curves that could be analyzed. The normalized curves were way too steep after normalization due to the steep background curves, so the halftime couldn't be properly retrieved.

We decided to instead take the non-normalized data for analyzing the recovery halftime. We also observed a strange drop in intensity for all collected data at around 55 seconds (data was recorded for 92 seconds), so we cut all data at this time. The analysis resulted in the following data for halftime against radius for FRAP on top of the hemispheres (*Table 3.2*):

Radius [µm]	5	7	10	14	17.5	20
# of measurements	5	4	5	3	3	3
Recovery halftime [s]	6.55	9.22	8.51	12.01	12.03	12.98
Standard Error	1.37	0.58	1.20	3.53	1.69	1.85

Table 3.2: Table summarizing the analyzed data form the FRAPs on the top of different sized hemisphere structures. Originally 6 measurements were done on each hemisphere size, but many measurements had to be discarded due to the rapid bleaching that took place.

The data from *Table 3.2* is displayed graphically in *Figure 3.8* below. The data is much rougher than the data presented in *Figure 3.3*, but overall the same trend is observed (roughly). We again find slower recovery in the larger structures and observe the same saturation effect.

Due to the poor quality of the data as a result of not being able to normalize the data, no further analysis was done.

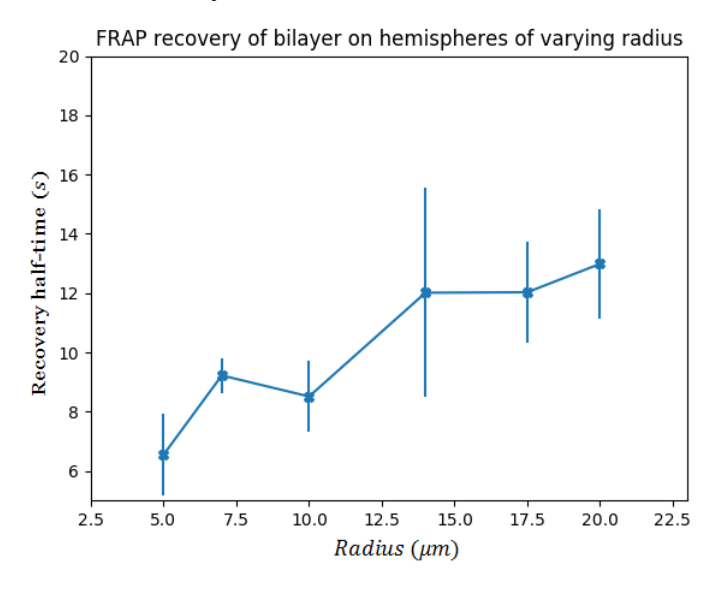


Figure 3.8: Halftime recovery of FRAP against radius of hemispheres.

3.2 Part 2: Colloid mobility

The realization of the setup presented in *Figure 2.1b* is a many step process, as described in *section 2.3*. The aim of the setup is to have a functional system of freely diffusing colloidal particles confined to a substrate with controllable curvature, so that their curvature-influenced motion can be studied. The following three criteria must thus be met for the setup to be considered functional:

- 1. Colloids must be mobile on a substrate
- 2. Colloids must be successfully linked to the substrate
- 3. Colloids must move on the substrate unaffected by gravity

In this section we present the steps we took in developing the system to meet the above criteria. Development has reached a point where we believe that it can be used for data collection shortly. The starting point of development was the setup shown in *Figure 2.1a*, as we found a mobile bilayer on the substrate to be a critical condition for mobile colloids.

In the tables below we show the different steps taken in development and whether or not we observed the colloids to be mobile under the circumstances. *Table 3.3* shows results without addition of complementary DNA, *Table 3.4* shows results where DNA was added.

Table 3.4 shows results where DNA was added. *Table 3.3:* Table summarizing the mobility of different colloids on different substrates. The mobile section indicates whether or not the colloids were mobile on the substrate.

Colloid Material	Size	Substrate	Mobile?	Comment
Silica	2.06µm	Glass	Yes	
Silica	0.91µm	Glass	Yes	
Silica	2.06µm	ORMOCER	Yes	
Silica	2.06µm	Nanoscribe Structures	Yes	
Polystyrene	0.9µm	Glass	No	Silica coating to solve problem
Silica coated	1µm	Glass	Yes	
polystyrene	1,000	Giass	165	
Silica coated	1,,,,,,	Nanoscribe	No	Bilayer on structure
polystyrene	$1\mu m$	Strucures	INO	showed poor mobility

32 Results

Table 3.4: Table summarizing results for Silica and Silica coated polystyrene col-
loids on glass, with added DNA linkers

Colloid	Size	Substrate	Mobile?	Comment
Silica	2.06µm	Glass Yes		Excess of DNA
Silica	2.00μπ	Glass	ies	decreased mobility
Silica coated	1 11111	Glass	No	Bilayer on glass
				showed poor
polystyrene	,			mobility

Colloids were classified to be mobile when over 90% of the particles showed clear brownian motion. Classifying samples as mobile or immobile involved little debate, as immobility of colloids was always a very clear situation where little to none of the colloids would move.

For the 2.06µm colloids we observed mobility at every stage of preparing the setup. These particles were too heavy however, so that criteria 3 was not satisfied. Determining whether they were linked to the substrate after adding DNA was therefore not easy to see, but excess addition of DNA decreased the number of mobile particles indicating that links were in fact established.

Silica coated polystyrene particles were light enough to not be affected by gravity, but appeared immobile on the structures or after DNA addition. We are unsure about the cause of this observation, but we also found poor bilayer mobility on the substrate for these samples which could be probable cause.

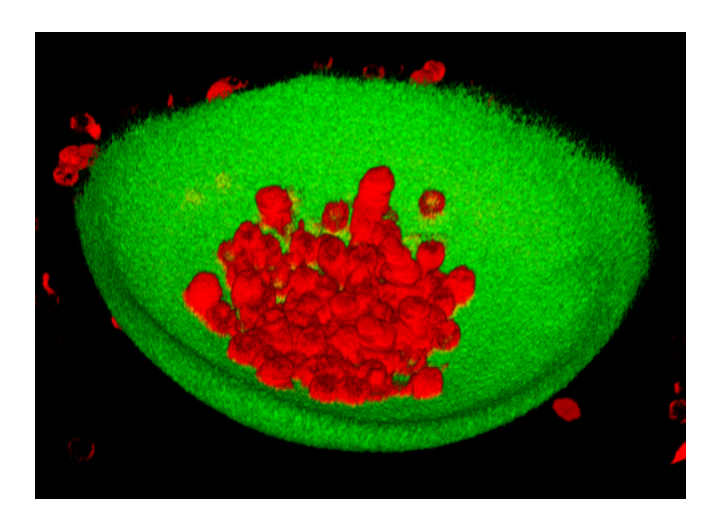
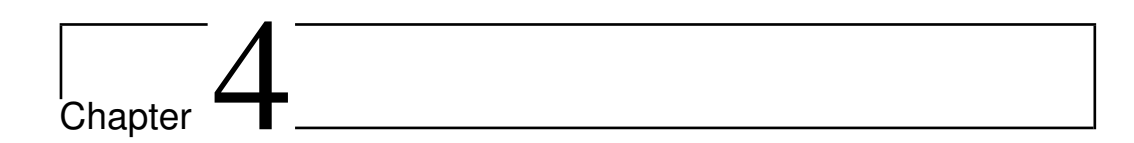


Figure 3.9: Fluorescence image of $2\mu m$ silica particles inside a $20\mu m$ inverted hemisphere structure.

A fluorescent image of $2\mu m$ silica particles inside the inverted hemisphere structure is seen in *Figure 3.9*. The silica particles were mobile, but all remained in the bottom of the hemisphere due to gravity. We believe that we should see the same mobility for the silica coated polystyrene particles, which should not be affected by gravity due to being much lighter. At this point the setup would be ready for collecting data on the motion of the colloids.



Conclusion

Following recent developments on the model of the cell membrane, we have developed an artificial cell membrane system to investigate the role of curvature on lipid and protein motion. Our system consists of a solid supported lipid bilayer on 3D printed hemispherical micro-structures, combined with DNA-linked colloid particles. We have used this system to observe the effect of curvature on the motion of a field of lipids. Furthermore we have developed the system to the point where we can soon observe the motion of colloids confined to our structures, uninfluenced by gravity.

Regarding the motion of lipids we used fluorescence recovery after photobleaching to determine the diffusion coefficient of lipids in bilayers on hemispherical structures of varying radii. A theoretical prediction for the effect of curvature on diffusion of a field of lipids on a sphere has been derived in two separate ways. Comparing the predicted trend to our collected data shows reasonable agreement between the data and the theoretical model. Applying the model to the data allows for a prediction to be made about the value of D_{flat} . This gave a value that corresponded with previously determined values, further indicating the suitability of the model. For further testing of the model however an actual value for D_{flat} on the material of our structures should be determined.

Regarding the motion of protein we have build a system with mobile silica particles linked with DNA to a bilayer on printed micro structures. We have observed our system to be functional for $2\mu m$ silica particles inside inverted hemispherical structures. We believe this system will also work with lighter colloidal particles, so that the motion of colloids on curved surfaces can soon be studied.

36 Conclusion

Experiments using homemade polystyrene particles were not yet successful, however new polystyrene particles have been ordered that have previously shown promising results. Homemade silica coated particles did show promising results, but more work is needed before we can say that they are suitable for the experiment.

In future work we believe it is definitely worthwhile to continue developing the DNA-linked colloidal system, with the aim of investigating motion of colloids on curved surfaces. Furthermore our system can be used to continue the investigation of lipid motion, by repeating the investigation on other geometries. We would like to start soon with cylinders and saddles, which have respectively a Gaussian and mean curvature of zero.



Acknowledgments

I would like to thank my supervisors Melissa Rinaldin and Daniela Kraft for their guidance and support throughout this bachelor project. I would like to especially thank Melissa for her help with writing and correcting this thesis and her readiness to provide me with all the technical support I needed during my project. Furthermore I want to thank Piermarco for providing a theoretical model that we could use to model our data and to thank Ruben Verweij for his help with the programming and data analysis. Lastly I would like to thank the entire soft-matter group for providing me with a great introduction to being part of a physics research group and for a great insight into the conducting of research within soft matter physics.

Bibliography

- [1] C. O' Connor and J. Adams, Essentials of Cell Biology, Cambrigde, 2010.
- [2] S. J. Singer and G. L. Nicolson, *The Fluid Mosaic Model of the Structure of Cell Membranes*, Science **175**, 720 (1972).
- [3] G. L. Nicolson, *The Fluid Mosaic Model of Membrane Structure: Still relevant to understanding the structure, function and dynamics of biological membranes after more than 40 years*, Biochimica et Biophysica Acta Biomembranes **1838**, 1451 (2014).
- [4] H. C. Lai and L. Y. Jan, *The distribution and targeting of neuronal voltage- gated ion channels.*, Nature reviews. Neuroscience 7, 548 (2006).
- [5] J. M. Chalovich and E. Eisenberg, *NIH Public Access*, Biophysical Chemistry **257**, 2432 (2005).
- [6] J. Zimmerberg and M. M. Kozlov, *How proteins produce cellular mem-brane curvature.*, Nature reviews. Molecular cell biology **7**, 9 (2006).
- [7] C. Cobbold, A. P. Monaco, A. Sivaprasadarao, and S. Ponnambalam, *Aberrant trafficking of transmembrane proteins in human disease*, Trends in Cell Biology **13**, 639 (2003).
- [8] A. Frost, V. M. Unger, and P. De Camilli, *The BAR Domain Superfamily: Membrane-Molding Macromolecules*, Cell **137**, 191 (2009).
- [9] C. Prévost, H. Zhao, J. Manzi, E. Lemichez, P. Lappalainen, A. Callan-Jones, and P. Bassereau, *IRSp53 senses negative membrane curvature and phase separates along membrane tubules.*, Nature communications **6**, 8529 (2015).

40 BIBLIOGRAPHY

[10] M. Adrian, R. Kusters, C. J. Wierenga, C. Storm, C. C. Hoogenraad, and L. C. Kapitein, *Barriers in the brain: resolving dendritic spine morphology and compartmentalization*, Frontiers in Neuroanatomy 8, 1 (2014).

- [11] D. Holcman and Z. Schuss, *Diffusion laws in dendritic spines*, The Journal of Mathematical Neuroscience **1**, 10 (2011).
- [12] S. Aimon, A. Callan-Jones, A. Berthaud, M. Pinot, G. E. Toombes, and P. Bassereau, *Membrane Shape Modulates Transmembrane protein Distribution*, Biophysical Chemistry **34**, 13 (2012).
- [13] A. Einstein, On the Motion of Small Particles Suspended in a Stationary Liquid, as Required by the Molecular Kinetic Theory of Heat, Annalen der Physik **322**, 549 (1905).
- [14] S. Paquay and R. Kusters, *A Method for Molecular Dynamics on Curved Surfaces*, Biophysj **110**, 1226 (2016).
- [15] R. P. Richter, R. Bérat, and A. R. Brisson, Formation of solid-supported lipid bilayers: An integrated view, Langmuir 22, 3497 (2006).
- [16] J. N. Israelachvili, D. J. Mitchell, and B. W. Ninham, *Theory of self-assembly of lipid bilayers and vesicles*, BBA Biomembranes **470**, 185 (1977).
- [17] I. Brouwer, A. Giniatullina, N. Laurens, J. R. T. van Weering, D. Bald, G. J. L. Wuite, and A. J. Groffen, *Direct quantitative detection of Doc2b-induced hemifusion in optically trapped membranes*, Nature Communications **6**, 8387 (2015).
- [18] D. Everett, *Basic principles of colloid science*, Royal society of chemical paperbacks, 1988.
- [19] V. Prasad, D. Semwogerere, and E. R. Weeks, *Confocal microscopy of colloids*, Journal of Physics: Condensed Matter **19**, 113102 (2007).
- [20] J. W. Lichtman and J. A. Conchello, *Fluorescence microscopy*, Nature Methods **2**, 910 (2005).
- [21] K. R. Spring and M. W. Davidson, *Introduction to fluorescence microscopy*, 2016.
- [22] MDougM, Fluorescence recovery after photobleaching, 2008.

BIBLIOGRAPHY 41

[23] D. Axelrod, D. E. Koppel, J. Schlessinger, E. Elson, and W. W. Webb, *Mobility measurement by analysis of fluorescence photobleaching recovery kinetics*, Biophysical Journal **16**, 1055 (1976).

- [24] K. Miura, EBML Lecture: What do FRAP curves tell us?, EMBL, 2015.
- [25] E. J. Vegter, C. V. D. Wel, and D. Kraft, Two Dimensional Diffusion of Colloidal Particles on Supported Lipid Bilayers, (2015).
- [26] H. Pandey, R. Rani, and V. Agarwal, *BRAZILIAN ARCHIVES OF BI-OLOGY AND TECHNOLOGY Liposome and Their Applications in Cancer Therapy Human & Animal Health*, Arch. Biol. Technol. v. Arch. Biol. Technol. v **5959**, 16150477 (2016).
- [27] S. van der Meulen, *How surface movile DNA linkers affect colloidal self-assembly*, PhD thesis, TU Delft, 2016.
- [28] Avanti, Avanti Polar Lipids.
- [29] I. Chakraborty, V. Meester, C. van der Wel, and D. J. Kraft, *Colloidal joints with designed motion range and tunable jointflexibility*, arXiv **1610.04018** (2016).
- [30] C. Graf, D. L. J. Vossen, A. Imhof, and A. Van Blaaderen, *A general method to coat colloidal particles with silica*, Langmuir **19**, 6693 (2003).
- [31] H. B. J. J. Salaris, M. Rinaldin, C. V. D. Wel, D. Kraft, and M. V. Hecke, On Modeling Protein Diffusion: Mobility of Colloidal Particles on Supported Lipid Bilayers, (2016).